Intra-winter atmospheric circulation changes over East Asia and North Pacific associated with ENSO in a seasonal prediction model

Sunyong Kim

Ocean Science and Technology School

Department of Convergence Study on the Ocean Science and Technology

Intra-winter atmospheric circulation changes over East Asia and North Pacific associated with ENSO in a seasonal prediction model

계절예측시스템을 이용한 엘니뇨와 관련된 동아시아-북태평양의 겨울내 대기순환 변동 분석

본 논문을 김선용의 이학석사 학위논문으로 인준함.

위원장 이 재 학 (인)

위 원 이 호 진 (인)

위 원 김 형 석 (인)

위 원 국 종 성 (인)

2015년 2월

한국해양대학교 해양과학기술전문대학원

Contents

List of Figures

Abstract

Intra-winter atmospheric circulation changes over East Asia and North Pacific associated with ENSO in a seasonal prediction model

Sunyong Kim

Department of Convergence Study on the Ocean Science and Technology

Ocean Science and Technology School

Though tropical SST anomalies associated with El Niño change slowly during the mature phase of El Niño, the resultant extratropical teleconnection patterns are quite different with time. In this study, the intra-winter changes in the teleconnection pattern associated with El Niño are investigated using the NCEP reanalysis and observational data and the high-resolution seasonal prediction data. The observational analyses show that there are distinctively changes in the teleconnection pattern over the North Pacific within the winter. In the early winter (November-December) of El Niño years, there is a distinctive anomalous Kuroshio anticyclone, which is closely related to the East Asian climate. In January, in contrast, the Kuroshio anticyclone suddenly disappears and a strong cyclonic flow, which is

part of the Pacific-North American (PNA) teleconnection pattern, develops. It is suggested that the intra-winter changes are controlled by the relative roles of the equatorial central Pacific (CP) and western north Pacific (WNP) precipitation anomalies on the extratropical teleconnection over the North Pacific. On the other hand, the prediction data failed to capture the observed intra-winter changes in the teleconnection pattern, though the predictive skills for tropical SST and precipitation are high. It is revealed that this model's discrepancy in the extratropical teleconnection is partly originated from the failure in predicting the relative magnitude of CP and WNP precipitation anomalies. Further analyses on the ensemble spread of the prediction data support the relative roles of CP and WNP precipitation anomalies in affecting the extratropical circulation over the North Pacific.

Key words: ENSO, East Asia climate, teleconnection, GloSea5

1. Introduction

The El Niño-Southern Oscillation (ENSO) is a large-scale climate phenomenon in the tropical Pacific Ocean that extensively influences the global weather and climate (Bjerknes, 1969; Horel and Wallace, 1981). The tropical sea surface temperature (SST) variations alter the mid-latitude climate through the atmosphere-ocean interaction and tropics-mid-latitude teleconnection (Hoskins and Karoly, 1981; Trenberth et al., 1998; Wang and Fu, 2000; Wang et al., 2000; Diaz et al., 2001; Ashok et al., 2007; Kug et al., 2009; Yeh et al. 2014). Thus far, many studies have investigated the relation between the tropical Pacific Ocean SST variation and the mid-latitude systems. In particular, El Niño is known to have direct and indirect influences on the climate in East Asia, including East China, Korea, and Japan via the teleconnection (Nitta, 1987; Ha, 1995; Ahn et al., 1997; Kang, 1998; Yang and Lau, 1998; Cha et al., 1999; Wu et al., 2003; Kug et al., 2010; Lim and Kim, 2013; Zhou et al., 2014). The East Asian climate is affected by several dynamic factors, not only by the tropical Pacific Ocean SST but also by the internal atmospheric variability and other climate phenomena. In this sense, there is still a large uncertainty in understanding the dynamical processes on impact of El Niño.

Wang et al. (2000) suggested a dynamical process on how the ENSO can affect East Asian climate. They suggested that the anticyclonic flow develops in the Philippine Sea during the boreal winter of El Niño phase. This anticyclone induces a southerly wind and transports the warm and moist air toward East Asia. As a result, the precipitation and temperature increase over East Asia. Wang et al. (2000) also pointed out that the Philippine Sea anticyclone moves northeast by the air-sea interaction in the western North Pacific (WNP) and is sustained until the following year summer, i.e., the El Niño mature phase, continuously

influencing the East Asian climate. As well as the local air-sea interaction, the Philippine Sea anticyclone can be intensified from the impact of the Indian Ocean SST warming (Watanabe and Jin, 2002; Xie et al., 2002; Lau and Nath, 2003; Kug and Kang, 2006; Kug et al., 2006a,b; Yang et al., 2007; Yuan et al., 2012). Recently, it is suggested that the Philippine Sea anticyclone can be understood as a result of the nonlinear interaction between the annual cycle and the ENSO mode (Stuecker et al., 2013).

Although the Philippine Sea anticyclone plays a quite important role in the relation between the ENSO and East Asian climate system, Son et al. (2014) emphasized that it is insufficient to explain the East Asia connection by the Philippine Sea anticyclone only. For example, the Philippine Sea anticyclone is confined in the subtropics, making it difficult to impact the mid-latitude region north of 30°N. Son et al. (2014) suggested that in addition to the Philippine Sea anticyclone the Kuroshio anticyclone, located in the North Pacific, significantly affects the climate variability in East Asia, covering East China, Korea, and Japan. They further emphasized that the Kuroshio anticyclone exists in November and December; but it suddenly disappears in January. The development and sudden decay of the Kuroshio anticyclone significantly influences the relation between El Niño and East Asian climate.

Son et al. (2014) suggested the El Niño teleconnection processes through the observational analyses and linear baroclinic model (LBM) experiments. It is known that anomalous diabatic cooling due to the suppressed convective heating over the WNP is responsible for developing the Philippine Sea anticyclone in the lower troposphere and the cyclonic flow in the upper troposphere. The upper level cyclonic flow leads to the extratropical anticyclone via the Rossby wave energy propagation, which is a key process in the development of Kuroshio anticyclone. At the same time, the positive precipitation anomalies over the equatorial central Pacific (CP) can lead to the Pacific North America

(PNA) pattern, which is linked to the overall cyclonic flow over the North Pacific (Ratnam et al., 2010). Therefore, the cyclonic flow induced by the positive precipitation over the equatorial CP competes with the anticyclonic flow induced by the negative precipitation over the WNP. Son et al (2014) argued that the Kuroshio anticyclone exists in the early winter due to the relatively strong WNP negative precipitation anomalies. However, in January, the Kuroshio anticyclone suddenly disappeared because the weakened negative precipitation anomalies over the WNP cannot beat the effect of positive precipitation anomalies over the equatorial CP.

Though Son et al. (2014) showed the observed evidences on the dynamical processes reasonably, their study has limitations due to their relatively shorter data sample. The seasonal prediction data will be a good test bed to evaluate this observational hypothesis. The objective of this study is to support the observational argument by analyzing the high resolution seasonal prediction data. Particularly, the compensating role between the WNP and the equatorial CP precipitation anomalies in the development and sudden extinction of the Kuroshio anticyclone will be intensively examined. At the same time, we can evaluate how well the current operational climate model simulates the observed teleconnection associated with El Niño.

Section 2 describes the observational data and the seasonal prediction data. In order to verify the seasonal prediction skill, the relationship between the observational data and simulation is included in Section3, and the teleconnection dynamics toward East Asia associated with ENSO is suggested in Section 4. Section 5 investigates the teleconnection difference from each ensemble spread consisting of the 12 members. The chapter ends in Section 6 with a summary and discussion including the implications of this study.

2. Data and model

2.1 GloSea5 model

Global Seasonal Forecast System version 5 (GloSea5) is the newest seasonal prediction model with a higher horizontal resolution version than the previous version (GloSea4) by the United Kingdom the Met Office (MacLachlan et al., 2014). This model is based on the HadGEM3 coupled model from the Met Office, and HadGEM3 is composed of the atmosphere model from MetUM (Met Office Unified Model; Walters et al., 2011), ocean model from NEMO (Nucleus for European Modeling of the Ocean; Madec, 2008), sea ice model from CICE (The Los Alamos Sea Ice Model; Hunke and Lipscomb, 2010) and land surface model from JULES (Joint UK Land Environment Simulator; Best et al., 2011). The horizontal resolution has increased by 0.833°×0.556° in the atmosphere and land surface model. Also, the grid in the ocean and the sea-ice model has improved from 1° to 0.25°. The ocean and sea-ice model are initialized by using the three-dimensional ocean data assimilation of NEMO (Mogensen et al., 2012), the new data assimilation system that uses identical resolution and physical parameterization.

The seasonal prediction data used in this study is produced by the Korea Meteorological Administration at the work-site operation in 2013. During the work-site operation period, GloSea5 hindcast is implemented for model climatological value and verification. The hindcast is carried out for 14 years from 1996-2009. It consists of 12 ensemble members, which are obtained from four different starting dates (1, 9, 17 and 25 of September) with the 3 different initial conditions. In this study we use the monthly mean forecast data in November, December and January to analyze the intra-winter changes in the teleconnection patterns.

2.2 Reanalysis and Observation data

The observation data for the atmospheric circulation is obtained from the monthly mean National Centers for Environmental Prediction/the National Center for Atmospheric Research (NCEP/NCAR; Kalnay et al., 1996) reanalysis data in order to compare with the seasonal prediction data. The grid spacing in the reanalysis data is a 2.5 ° latitude-longitude resolution, and the dataset used is from 1996 to 2009. For the precipitation monthly mean CPC Merged Analysis of Precipitation (CMAP; Xie and Arkin, 1997) data is used with the same resolution and the period. Also, NOAA Extended Reconstructed SST version 3 (ERSST.v3d; Smith et al., 2008) is analyzed for the tropical Pacific SST variation.

3. Verification of the prediction skill

Before we analyze the dynamical processes using the forecast data, the prediction skill of GloSea5 is investigated. Figure 1 shows the correlation skill of Niño3 (150 ° W-90 ° W, 5 ° S-5 ° N), Niño3.4 (170 ° W-120 ° W, 5 ° S-5 ° N) and Niño4 (160 ° E-150 ° W, 5 ° S-5 ° N) SST, respectively. Though the correlation skill rapidly decreases after March, possibly due to the spring predictability barrier (SPB; Webster and Yang, 1992; Chen et al., 1995; Webster, 1995; Chen et al., 2004; Jin et al., 2008; Duan and Wei, 2013), GloSea5 shows a quite high skill with more than 0.9 correlation during the boreal winter. This indicates that the model prediction captures the El Niño variability quite well during the boreal winter time, which is the target period for the analyses. The anomaly correlation is higher than the persistence for the three indices though it becomes lower from February prediction.

In addition to the El Niño indices, GloSea5 reasonably predicts the SST pattern. Figure 2 shows the correlation skill for the tropical SST. As seen in Figure 1, GloSea5 exhibits a very high correlation over the equatorial central and the eastern Pacific. Though the correlation is relatively lower than those of the equatorial central and the eastern Pacific, GloSea5 also estimates the significant correlation in the WNP from November to December. Interestingly, the forecast skill in January is higher than that in November over the WNP in spite of the longer lead time. In addition, the skill over the Indian Ocean is also quite high.

In order to understand the extratropical teleconnection pattern, it is important to know how well the model predicts the tropical precipitation. To evaluate this, the correlation skill for the precipitation is calculated from GloSea5. As shown in Figure 3, GloSea5 has a high prediction skill over the equatorial central and the eastern Pacific. It is also noted that there is a significant correlation over the WNP, whose precipitation variability is quite important for

the developing Kuroshio anticyclone. It is interesting that there is a significant skill over East Asia in November and January. Son et al. (2014) showed that the precipitation variability in the Korean Peninsula is highly correlated with the El Niño index in November and December, but their relation is weakened in January. This significant skill in East Asia can be a result of its close relation with ENSO, which will be discussed below. In addition, there is also a significant prediction skill over the Indian Ocean. The SST and the precipitation variability over the Indian Ocean are affected by the El Niño phase (Klein et al., 1999; Webster et al., 1999; Ashok et al., 2001; Lau and Nath, 2003; Xie et al., 2002; Kug et al., 2004, 2005). So far, we showed that the model has a good skill where the El Niño-related signal is strong in the observation. This suggests that the model has the ability to simulate the observed El Niño patterns and can provide a good test bed to evaluate the observational hypothesis on the intra-winter changes in the El Niño teleconnection to East Asia.

4. Teleconnection over East Asia and North Pacific

Prior to showing the teleconnection pattern from the model prediction, the observational teleconnection pattern associated with El Niño is calculated. For this, the linear regression of the wind and geopotential height anomalies at 850-hPa and 500-hPa with respect to the Niño3 SST are shown in Figure 4. Son et al. (2014) already showed a similar analysis, but in this study we only used the data from 1996/1997 to 2009/2010 in order to directly compare it with the prediction result.

In November, the anticyclonic flow over the Philippine Sea exists at both 850-hPa and 500-hPa (Figure 4a, b). The anticyclone is stronger in the lower level, supporting that the Philippine Sea anticyclone is a part of the response to anomalous diabatic heating related to the negative precipitation anomaly (Wang et al. 2000). This Philippine Sea anticyclone can lead to the anomalous southerly wind along the coastal line of the Eurasian Continent in the subtropics. In addition to the Philippine Sea anticyclone, there is a distinctive anticyclone over the Kuroshio expansion region. This Kuroshio anticyclone signals are clearly shown in both 850-hPa and 500-hPa field, but it is stronger at 500-hPa unlike the Philippine Sea anticyclone. It is evident that the strong southerly wind exists in the western part of the Kuroshio anticyclone, including the Korea Peninsula and Japan, which affects the climate variability. On the other hand, the cyclonic flow exists in the eastern part of the North Pacific. Until November, the zonal scale of this cyclonic flow is relatively small, and its magnitude is relatively weak.

In December, the Philippine Sea anticyclone moves eastward but the magnitude is maintained. The Kuroshio anticyclonic flow also tends to move slightly westward. In addition, the center is shifted to the south compared to that in November. Therefore, the southerly wind

is intensified over the Korean Peninsula and Japan. On the other hand, the cyclonic flow near the North America is reinforced and stretches out westward in high latitude around 50 ° N. It seems that the southward shift of the Kuroshio anticyclone region is related to the westward expansion of the cyclonic flow. Interestingly, it is noted that the distinctive cyclonic flow prevails over the Eurasian Continent. In addition to the Kuroshio anticyclone, this cyclonic flow plays an essential role in strengthening the southerly wind in East Asia.

Atmospheric circulation in January shows dramatic changes compared to that in November and December (Figure 4e, f). In the tropics, the Philippine Sea anticyclone widens eastward in the lower level. In addition, the meridional extent of the Philippine Sea anticyclone is exceedingly expanded. At 500-hPa, there is an overall anticyclonic flow in the subtropical region. As suggested in Son et al. (2014), the Kuroshio anticyclone suddenly disappears in January and a weak cyclonic flow is found over East Asia. While the Philippine Sea anticyclone induces southerlies confined in the subtropics, the weak northerlies exist over East Asia. The change of the anomalous wind direction from December to January results in dramatic intra-winter changes in the relationship between ENSO and the East Asian climate (Son et al. 2014).

On the other hand, the north Pacific cyclonic flow explosively develops in comparison with that in December. This cyclonic flow can be interpreted as a part of the PNA pattern, explained by the forced Rossby wave response to the equatorial diabatic heating associated with El Niño, which affects the North American climate (Hoskins and Karoly, 1981). Previous studies pointed out that the intensity of the PNA pattern response is stronger in the late winter period (Livezey and Mo, 1987; Livezey at al., 1997; Wang and Fu, 2000; Blade et al., 2008). It is conceived that the abrupt decay of the Kuroshio anticyclone is closely connected to the explosive development and westward expansion of the anomalous cyclonic flow over the north Pacific region. Interestingly, the distinct cyclonic flow located in the

Eurasian continent no longer exists in January. This rapid change of the atmospheric circulation over Eurasian Continent during the El Niño events should be further studied.

So far, we showed intra-winter changes in the El Niño teleconnection patterns from the observations, which show dramatic changes between December and January. The overall features are quite consistent with the findings of Son et al. (2014), indicating the robustness to the analyzing period. Next, in order to support the observational argument and to assess the models' ability, we checked the same teleconnection patterns from the GloSea5 prediction data (Figure 5). It is clear that GloSea5 reasonably simulates the Philippine Sea anticyclone in the lower level in November (Figure 5a). However, the model tends to underestimate the strength of Kuroshio anticyclone compared to the observation data. The anticyclonic flow exists weakly at 500-hPa with its location being shifted westward, and is even invisible at 850-hPa. Alternatively, the north Pacific cyclonic flow is stronger than that in the observation data in November.

In December, the Philippine Sea anticyclone evolves eastward, consistent with the observation. The Kuroshio anticyclone is enhanced in December compared to November, but in general it is still smaller and weaker than in the observation. The Kuroshio anticyclonic flow exists in both vertical levels, so that the southerly wind exists in East Asia. The precipitation prediction skill over East Asia showed in Figure 3a, b can be linked with the southerly wind. It is also noted that the dominant cyclonic flow over the north Pacific is further enhanced in December, which is still stronger than the observational one (Figure 5c, d).

Consistent with the observation, the Kuroshio anticyclone is weakened in January compared to that in December, but the anticyclonic flow still exist in January unlike the observation. This indicates that the prediction model fails to simulate the observed sudden disappearance of the Kuroshio anticyclone, though the magnitude of the anticyclone becomes

weaker than in December. This means that GloSea5 has problems in simulating teleconnection pattern and the related impacts associated with ENSO.

Son et al. (2014) suggested that the development and sudden dissipation of the Kuroshio anticyclone are closely connected to the tropical precipitation pattern associated with ENSO. During the El Niño events, positive precipitation anomalies occur in the equatorial CP, shifting the strong convective activity toward the equatorial CP. Almost concurrently, the negative precipitation anomalies arise with relatively suppressed convection in the equatorial western Pacific. The anomalous diabatic cooling due to the weak convection over the WNP induces a cyclonic flow in the upper level and the Philippine Sea anticyclone in the lower level (Gill, 1980). The upper level cyclonic flow over the WNP leads to the anticyclone in the mid-latitudes through a Rossby wave energy propagation (Hoskins and Karoly, 1981). The Kuroshio anticyclone can be explained by the forced Rossby wave response from the tropical diabatic cooling. In the mid-latitudes, the upper level anticyclone induces the anticyclonic flow in the lower level, maintaining the barotropic structure. During the boreal winter, particularly in the El Niño peak phase, this anticyclone intensely affects the climate in East Asia, including Korean, Japan and the northeastern China region.

On the other hand, the intensification of the convective activity in the equatorial CP leads to the anomalous cyclonic flow in the north Pacific via a PNA-like pattern and ultimately plays a role in suppressing the Kuroshio anticyclone. According to these dynamical processes, the strength and extinction of the Kuroshio anticyclone during the El Niño events is determined by the relative magnitude of both the convection decrease in WNP and the convection increase in the equatorial CP. In other words, the Kuroshio anticyclone develops in December because of the relatively stronger effect of the negative precipitation anomaly over the WNP. On the other hand, in January the negative precipitation anomalies in the WNP become weaker and the positive precipitation anomalies in the equatorial CP become stronger.

In addition, the climatological easterly vertical shear is stronger over the equatorial CP in January than in December, meaning that the upper level response to the equatorial diabatic heating over CP is stronger, which leads to a stronger extratropical teleconnection. Therefore, the abrupt disappearance of the Kuroshio anticyclone in January is due to the dominant effect of positive precipitation anomalies in the equatorial CP (Son et al. 2014).

Based on these dynamical processes, we may evaluate why the prediction data failed to simulate the teleconnection patterns. So, the precipitation pattern of ENSO teleconnection is compared between the observation data and the GloSea5 prediction data (Figure 6). The observational patterns exhibit the typical precipitation features during the El Niño peak phase such as the positive precipitation anomalies in the equatorial CP and the negative precipitation anomalies in the WNP. Even though the SST patterns do not change much within winter (November to January), the tropical precipitation exhibits the significant intra-winter changes. Compared to the anomalies in December, the negative precipitation in the WNP sharply decreases in January, whereas the positive precipitation in the equatorial CP tends to increase with the southward shift. These features are also reported in Son et al. (2014), though their analyzing period is different.

As expected from the correlation skill of the precipitation shown in Figure 3, GloSea5 captures the general patterns of the negative precipitation in the WNP and the positive precipitation in the equatorial CP (Figure 6a, c, e). However, it is clear that GloSea5 failed to simulate the observed intra-winter changes in the precipitation patterns. The WNP precipitation, for instance, is weaker than the observed in December (Figure 6c), but stronger in January (Figure 6e). Therefore, it seems the prediction data failed to simulate the observed sudden decrease of WNP precipitation from December to January. On the other hand, the anomalous positive precipitation in the equatorial CP becomes weaker in January (Figure 6e). These discrepancies may result in the different teleconnection pattern from the observation.

In order to investigate the relative precipitation magnitude between the observation data and GloSea5, the differences in the regression pattern of the precipitation are calculated (Figure 7). In November and December, both the WNP and the equatorial CP indicate a positive precipitation difference (Figure 7a, b). The positive precipitation difference means that GloSea5 simulates the WNP negative precipitation weaker and the CP positive precipitation stronger. The weaker negative precipitation over the WNP is related to weaker simulation of the Kuroshio anticyclone via the teleconnection pattern toward the mid-latitude. The overestimation of the equatorial CP precipitation also leads to the stronger cyclonic flow in the north Pacific. This plays a dominant role in weakening the Kuroshio anticyclone (Figure 5b, d).

In contrast to the case in November and December, the precipitation difference in January (Figure 7c) shows somewhat a different pattern. There is the negative difference over the WNP, which indicates that the prediction data overestimates the strength of the negative precipitation in January. This plays a role in maintaining the Kuroshio anticyclone in the model prediction, different from the observed evolution. Also, the precipitation differences between January and December in the prediction and the observation data are calculated in Figure 8. The positive (negative) precipitation difference indicates that the precipitation in January is stronger (weaker) than in December. Both data exhibits similar results, the positive precipitation over the WNP and the negative precipitation over the equatorial CP. This means that the negative precipitation over the WNP in January is stronger than in December, but the positive precipitation over the equatorial CP is opposite.

In order to clearly compare the magnitude of the WNP (110 ° E-150 ° E, 0 ° N-10 ° N) and the equatorial CP precipitation (180 ° E-130 ° W, 5 ° S-5 ° N), the area-averaged precipitation anomaly in the observation and GloSea5 prediction data are calculated (Figure 9). In the case of the WNP precipitation, GloSea5 simulates the weaker anomaly in November

and December. In particular, the simulated precipitation is smaller by about 44% than the observed value in December. On the other hand, in January, GloSea5 precipitation is even slightly stronger than the observed. In addition, it is clearly shown that the negative WNP precipitation anomalies remarkably drop from December to January in the observation data, while the prediction data exhibits the increasing trend of the negative precipitation from December to January. For the positive precipitation over the equatorial CP (Figure 9b), GloSea5 tends to overestimate the precipitation in November and December while underestimation is seen in January. In the observation, the area-averaged positive anomaly is slightly stronger in January but almost the same magnitude, though the maximum value of the precipitation anomalies as shown in Figure 6f is distinctively stronger. This is related to the southward shift of the precipitation pattern (Harrison and Vecchi, 1997). Though the magnitude of the precipitation is quite similar, their effect on the extratropical teleconnection can be considerably larger in January. Since the climatological easterly shear is the largest in January, the upper level response to the diabatic heating is stronger (Wang and Xie, 1996; Wang et al., 2000), leading to the stronger extratropical teleconnection response. GloSea5 shows substantial decline of the positive precipitation from December to January. This leads to relatively weaker intensification of the cyclonic flow over the North Pacific compared to the observation, which can partly contribute to the survival of the Kuroshio anticyclone in January.

5. Teleconnection difference from ensemble spread

So far, we showed the intra-winter changes in the El Niño teleconnection pattern based on the observation data and GloSea5 prediction data over 14 years. Clearly, the prediction data have discrepancies in predicting the teleconnection patterns on average, and these discrepancies can be explained by the dynamical process suggested by Son et al. (2014). In turn, these strong relationships between the biases in the tropical precipitation and extratropical relation support the observational hypothesis on the relative roles of the WNP and the equatorial CP precipitation. However, there is still a limitation due to the small sample size of 14 years. In order to make up for this issue, the individual ensemble members are analyzed. In the previous section, we showed the ensemble mean result based on the 12 individual ensembles. During the same El Niño years, the individual prediction members simulate the precipitation and the teleconnection pattern very differently. Therefore, the relation between the tropical precipitation and extratropical teleconnection patterns among individual ensembles will provide a good place to test the observational hypothesis. That is, we may check the relative roles of the WNP and equatorial CP precipitation in the evolution of the Kuroshio anticyclone based on the ensemble spread; since the dynamical process on the Kuroshio anticyclone, suggested by Son et al. (2014), should work on the individual ensemble members.

Before we check the WNP and the equatorial CP precipitation roles, the precipitation spread based on the 12 individual ensemble members is shown in Figure 10. The noise related in precipitation signal is in response to the SST. The precipitation over the WNP especially has strong discrepancies from November to January compared with the other area. This clearly means that each ensemble members in the prediction data diversely simulates the

precipitation in the WNP. So, the teleconnection pattern during El Niño towards East Asia can be different in each ensemble members because of the WNP precipitation response affecting the Kuroshio anticyclone.

In order to separate the relative roles of the WNP and the equatorial CP precipitation, we divided individual ensembles into two groups. Firstly, we selected the El Niño years, when the NIÑO3 SST is greater than its 0.5 standard deviation. Among the 14 prediction years from 1996 to 2009, total of 6 years were selected as the main El Niño years: 1997/1998, 2002/2003, 2003/2004, 2004/2005, 2006/2007, 2009/2010. As to each of the El Niño years, among the 12 ensemble members, some members were selected into two groups based on the WNP (110 ° E-150 ° E, 0 ° N-10 ° N) and equatorial CP precipitation (180 ° E-130 ° W, 5 ° S-5 ° N) in each month. One is for the strong negative precipitation in the WNP and the weak positive precipitation in the equatorial CP, compared with the ensemble mean precipitation anomaly in each region. The other had the opposite condition, the weaker negative precipitation in the WNP and the stronger positive precipitation in the equatorial CP than the ensemble mean precipitation anomaly. Hereafter, the former is designated as “strong WNP case” and the latter one is “strong CP case”.

Figure 11 shows the El Niño composites of the precipitation anomalies for the strong WNP case and the strong CP case. As expected, the strong WNP case is characterized by the strong negative precipitation in the WNP and the weak positive precipitation in the equatorial CP. On the other hand, the strong CP case shows the weak negative WNP precipitation and strong positive equatorial CP precipitation. The former can be linked to the observed December forcing, and the latter can be linked to the observed January forcing under the same basic states. Because the precipitation in the equatorial CP is a direct response to the SST warming, the inter-model spread is relatively small. The WNP precipitation, however, is

affected by the complex dynamics (e.g. Wang et al., 2000; Watanabe and Jin, 2003; Kug and Kang, 2006), and the ensemble spread is considerably large.

The teleconnection pattern will be determined by the tropical diabatic heating and tropical/extratropical background states at large extent. Based on the two groups, we may isolate the impact of the different tropical diabatic heatings on the teleconnection patterns by comparison in the same month. Figure 12 displays the teleconnection pattern at 850-hPa during the El Niño events between the two cases. In the strong WNP case, the Kuroshio anticyclone clearly exists in November (Figure 12a). Note that the ensemble mean result does not show the anticyclonic signal in East Asia (Figure 5a). In the strong CP case, it is evident that the cyclonic flow overwhelms the north Pacific while the Kuroshio anticyclone is hardly found (Figure 12b). In December, the anticyclonic flow exists in East Asia, and small-scale eddy structure prevails over the North Pacific, possibly due to the extremely strong negative WNP precipitation (Figure 12c). In the strong CP case, on the other hand, the cyclonic flow still overwhelms the North Pacific, and the anticyclone flow is weakly found in East Asia.

In January, the weak anticyclone flow is found in the western part of the North Pacific and the cyclonic flow is dominant over the North Pacific, where the strong WNP cases are composited (Figure 12e). In the strong CP case, the explosive cyclonic flow settles down over the whole North Pacific including East Asia (Figure 12f). It is quite interesting that the strength of the cyclonic flow becomes stronger in January than in December, though the positive precipitation is slightly weakened in the equatorial CP. This implies that the January basic state, like stronger easterly shear, induces stronger extratropical teleconnection responses. In addition, the weaker negative WNP precipitation in January plays a critical role in the strong development of the cyclonic flow. In summary, the strong WNP case consistently shows a relatively strong anticyclone flow near East Asia and a weak cyclonic flow over the North Pacific in the all months. Conversely, the strong CP case consistently

shows relatively strong cyclonic flow over the whole North Pacific, and hardly simulates the Kuroshio anticyclone. These results strongly support the relative roles of the WNP and the equatorial CP precipitation anomalies on the extratropical teleconnection over the North Pacific.

6. Climatological field in tropics and extratropics

Figure 13 shows the monthly mean precipitation climatology between the prediction and the observation data from 1996 to 2009. The overall precipitation pattern between the prediction and the observation data is similar. As compared with the observational climatology (Figure 13a, c, e), the precipitation pattern simulated in prediction appears to have a heavy precipitation in the tropical region including Indian and Pacific Ocean. Also, the observational precipitation tends to drop in January compared with the early winter time. In contrast to the precipitation in the observation data, the prediction overestimates the precipitation in the tropics.

The prediction data simulates well both 500-hPa (Figure 14) and 850-hPa (Figure 15) field as well as the precipitation. Since the climatological field in tropics and extratropics is practically the same as the observation, the fail in the teleconnection patterns using prediction model is not directly related to the mean atmospheric condition. It is noticeable that the great part of the teleconnection pattern can be explained by the negative precipitation anomalies over the WNP and the positive precipitation anomalies over the equatorial CP.

7. Summary and discussion

This study investigates the intra-winter changes in the atmospheric circulation over East Asia associated with the ENSO from the seasonal prediction data, which are operationally used in the Korea Meteorological Administration (KMA). We found here that the seasonal prediction data shows poor ability in predicting the extratropical teleconnection pattern associated with ENSO though the predictive skills for the tropical SST and the precipitation are quite high. In particular, the prediction model has a serious problem in simulating the strength of the Kuroshio anticyclone in early winter and the sudden decay in January. This study explores the reason that the prediction model failed to simulate the teleconnection pattern. In spite of the high correlation skill for the precipitation, the prediction model has poor ability in simulating the detail evolution of the WNP and the equatorial CP precipitation anomalies. First, the prediction model simulates weaker negative WNP precipitation in early winter, which is responsible for the weak Kuroshio anticyclone. Second, the prediction model does not simulate the weakening of the WNP precipitation from December to January, which is related to the sudden decay of the Kuroshio anticyclone. Third, the prediction model tends to simulate a decrease of the positive equatorial CP precipitation from December to January, which partly contributes to the persistent Kuroshio anticyclone in January.

These strong relationships between the biases in the tropical precipitation and the extratropical circulation in turn support the observational hypothesis on the relative roles of the WNP and the equatorial CP precipitation. This is further convinced from the analyses of the ensemble spread. It is shown that the extratropical teleconnection during the same El Niño year is quite different among the ensemble members, and the WNP and the equatorial CP

precipitation anomalies are important components in controlling the ensemble spread of the extratropical teleconnection. That is, the ensemble spread clearly supports the relative roles of the WNP and the CP precipitation anomalies on the extratropical teleconnection over the North Pacific.

The present results have two prominent implications. First, the hypothesis suggested in the observation data is confirmed by connecting the estimation problem in the tropical precipitation and the incorrect teleconnection. Second, the performance of the KMA operational seasonal prediction model in predicting the teleconnection is evaluated. Based on the relation between the tropical precipitation and teleconnection pattern simulated in the prediction model, the forecast skill for the extratropical regions can be improved using the statistical post-processing (e.g. Kug et al., 2008a, b). Furthermore, our analyses provide a direction on how the prediction model can be improved to have a better prediction skill in the extratropical region. In spite of these implications, this study can be extended further. So far, the available prediction data of GloSea5 is relatively short and our prediction results (e.g. systematic bias) might be dependent on the data period. The long-term hindcast data is needs to be evaluated the systematic bias in the tropical precipitation and the teleconnection pattern. In addition, our results are based on a single prediction model. The results can be model-dependent, more robust results can be obtained from a multi-model framework. In particular, since most CMIP5 climate models have a difficulty in simulating the Kuroshio anticyclone, the multi-model analyses can give an insight to what the commonly missing component of the state-of-the-art climate models is in simulating the El Niño teleconnection in the extratropics including East Asia.

CMIP5 multi-model ensemble analyses are not including in this paper, it also failed to simulate the teleconnection patterns. CMIP5 captures well the typical patterns of the negative precipitation in the WNP and the positive precipitation in the equatorial CP. However, the

WNP precipitation is considerably weaker than the observation. As a result, the Kuroshio anticyclone is continually weak in the early winter time. In January, the anomalous positive precipitation in the equatorial CP becomes stronger, in common with the observation data.

References

Ahn, J.-B., J.-H. Ryu, E.-H. Cho, J.-Y. Park, and S.-B. Ryoo, 1997: A Study on correlations between air-temperature and precipitation in Korea and SST over the Tropical Pacific. *J. Korean Meteor. Soc*., **33**, 487-495. (in Korean with English abstract)

Ashok, K., Z. Guan, and T. Yamagata, 2001: Impact of the Indian Ocean Dipole on the Relationship between the Indian Monsoon Rainfall and ENSO. *Geophys. Res. Lett.*, **28**, 4499-4502.

Ashok, K., S. K. Behera, S. A. Rao, H. Weng, and T. Yamagata, 2007: El Niño Modoki and its possible teleconnection. *J. Geophys. Res.*, **112**, C11007.

Best, M. J., et al., 2011: The Joint UK Land Environment Simulator (JULES), model description – Part 1: Energy and water fluxes, *Geosci. Model Dev.*, **4**, 677-699.

Blade, I., M. Newman, M. A. Alexander, J. D. Scott, 2008: The late fall extratropical response to ENSO: sensitivity to coupling and convection in the tropical West Pacific. *J. Clim*ate, **21**, 6101-6118.

Bjerknes, J., 1969: Atmospheric teleconnections from the equatorial Pacific. *Mon. Wea. Rev.*, **97**, 163-172.

Cha, E.-J., J.-G. Jhun, and H.-S. Chung, 1999: A study of characteristics of climate in South Korea for El Niño/La Niña years. *J. Korean Meteor. Soc*., **35**, 98-117. (in Korean with English abstract)

Chen, D., S. E. Zebiak, A. J. Busalacchi, M. A. Cane, 1995: An improved procedure for El Niño forecasting: Implications for predictability. *Science*, **269**, 1699-1702.

Chen, D., M. A. Cane, A. Kaplan, S. E. Zeblak, and D. Huang, 2004: Predictability of El Niño over the past 148 years. *Nature*, **428**, 733-736.

Diaz, H. F., M. P. Hoerling, and J. K. Eischeid, 2001: ENSO variability, teleconnections and climate change. *Int. J. Climatol.*, **21**, 1845-1862.

Duan, W., C. Wei, 2013: The 'spring predictability barrier' for ENSO predictions and its possible mechanism: results from a fully coupled model. *Int. J. Climatol.*, **33**, 1280-1291.

Gill, A. E., 1980: Some simple solutions for heat-induced tropical circulations. *Q. J. R. Meteorol. Soc*., **106**, 447-462.

Ha, K.-J., 1995: Interannual variabilities of wintertime Seoul temperature and the correlation with Pacific Sea surface temperature. *J. Korean Meteor. Soc*., **35**, 98-117. (in Korean with English abstract)

Harrison, D. E., and G. A. Vecchi, 1997: Westerly wind events in the tropical Pacific, 1986-95. *J. Climate*, **10**(12), 3131-3156.

Horel, J. D., Wallace, J. M., 1981: Planetary scale atmospheric phenomena associated with the Southern Oscillation. *Mon. Wea. Rev.*, **125**, 773-788.

Hoskins, B. J., and D. J. Karoly, 1981: The steady linear response of a spherical atmosphere to thermal and orographic forcing. *J. Atmos. Sci.,* **38**, 1179-1196.

Hunke, E. C. and Lipscomb, W. H., 2010: CICE: the Los Alamos Sea Ice Model Documentation and 15 Software User's Manual Version 4.1 LA-CC-06-012, T-3 Fluid Dynamics Group, Los Alamos National Laboratory, 2163.

Jin, E. K., J. L. Kinter, B. Wang, C.-K. Park, I.-S. Kang, et al., 2008: Current status of ENSO prediction skill in coupled ocean–atmosphere models. *Clim. Dyn.*, **31**, 647-664.

Kalnay, E., et al 1996: The NCEP/NCAR 40-year reanalysis project. *Bull. Amer. Meteoro. Soc.*, **77**, 437-471.

Kang, I.-S., 1998: Relationship between El Niño and climate variation over Korea peninsula. *J. Korean Meteor. Soc*., **34**, 390-396. (in Korean with English abstract)

Klein, S. A., B. J. Soden, and N.-C. Lau, 1999: Remote sea surface temperature variations during ENSO: Evidence for a tropical atmospheric bridge. *J. Climate*, **12**, 917-932.

Kug, J.-S., I.-S. Kang, J.-Y. Lee, and J.-G. Jhun, 2004: A statistical approach to Indian Ocean sea surface temperature prediction using a dynamical ENSO prediction. *Geophys. Res. Lett.*, **31**, L09212.

Kug, J.-S., S.-I. An, F.-F. Jin, and I.-S. Kang, 2005: Preconditions for El Niño and La Niña onsets and their relation to the Indian Ocean. *Geophys. Res. Lett.*, **32**, L05706.

Kug, J.-S., and I.-S. Kang, 2006: Interactive feedback between the Indian Ocean and ENSO. *J. Climate*, **19**, 1784-1801.

Kug, J.-S., T. Li, S.-I. An, I.-S. Kang, J.-J. Luo, S. Masson, and T. Yamagata, 2006a: Role of the ENSO-Indian Ocean coupling on ENSO variability in a coupled GCM. *Geophys. Res. Lett.*, **33**, L09710.

Kug J.-S., Ben P. Kirtman, and I.-S. Kang, 2006b: Interactive Feedback between ENSO and the Indian Ocean in an Interactive Coupled Model. J. Climate, 19, 6371-6381.

Kug, J.-S., I.-S. Kang, D.-H. Choi, 2008a; Seasonal climate predictability with Tier-one and Tier-two prediction systems. *Clim. Dyn*., **31**, 403-416.

Kug, J.-S., J.-Y. Lee, I.-S. Kang, B. Wang, C. K. Park, 2008b: Optimal multi-model ensemble method in seasonal climate prediction. *Asia-Pacific J. Atms. Sci.*, **44**, 233-247.

Kug, J.-S., Jin, F.-F., and An, S.-I., 2009: Two-types of El Niño events: Cold Tongue El Niño and Warm Pool El Niño. *J. Clim*ate, **22**, 1499-1515.

Kug, J.-S., M.-S. Ahn, M.-K. Sung, S.-W. Yeh, H.-S. Min, and Y.-H. Kim, 2010: Statistical relationship between two types of El Niño events and climate variation over the Korean Peninsula. *Asia-Pacific J. Atmos. Sci*., **46**(4), 467-474.

Lau, N.-C., and M. J. Nath, 2003: Atmosphere–Ocean Variations in the Indo-Pacific Sector during ENSO Episodes. *J. Climate*, **16**, 3-20.

Lim Y.-K., H.-D. Kim, 2013: Impact of the dominant large-scale teleconnections on winter temperature variability over East Asia. *J. Geophys. Res*., **118**(14), 7835-7848.

Livezey, R. E., and K. C. Mo, 1987: Tropical-extratropical teleconnections during the northern hemisphere winter. Part II: relationships between monthly mean northern hemisphere circulation patterns and proxies for tropical convection. *Mon. Weather Rev*., **115**, 3115-3132.

Livezey, R. E., M. Masutani, A. Leetmaa, H. Rui, M. Ji, and A. Kumar, 1997: Teleconnective Response of the Pacific–North American Region Atmosphere to Large Central Equatorial Pacific SST Anomalies. *J. Climate*, **10**, 1787-1820.

MacLachlan, C., et al., 2014: Global Seasonal forecast system version5 (GloSea5): a high-resolution seasonal forecast system, *Q. J. R.Meteorol. Soc*., doi:10.1002/qj.2396.

Madec G., 2008: NEMO Ocean Engine, Note du Pole de Modelisation. Institut Pierre-Simon Laplace (IPSL): Paris.

Mogensen, K., M. A. Balmaseda, A. T. Weaver, 2012: The NEMOVAR ocean data assimilation system as implemented in the ECMWF ocean analysis for System 4, Technical Report TR-CMGC-12-30. CERFACS: Toulouse, France.

Nitta T., 1987: Convective Activities in the Tropical Western Pacific and Their Impact on the Norther Hemisphere Summer Circulation. *J. Meteor. Soc. Japan*, **64**, 373-390.

Ratnam, J. V., S. K. Behera, Y. Masumoto, K. Takahashi, and T. Yamagata, 2010: Pacific Ocean origin for the 2009 Indian summer monsoon failure, *Geophys. Res. Lett.*, **37**, L07807.

Smith, T. M., R. W. Reynolds, T. C. Peterson, and J. Lawrimore, 2008: Improvements NOAAs Historical Merged Land–Ocean Temp Analysis (1880–2006). *J. Climate*, **21**, 2283-2296.

Son, H.-Y., J.-Y. Park, J.-S. Kug, J. Yoo, C.-H. Kim, 2014: Winter Precipitation variability over Korean Peninsula associated with ENSO. *Clim. Dyn.* **42**, 3171-3186.

Stuecker, M. F., A. Timmermann, F.-F. Jin, S. McGregor, H.-L. Ren, 2013: A combination mode of the annual cycle and the El Niño/Southern Oscillation. *Nature Geosci*., **6**, 540-544.

Trenberth, K. E., G. W. Branstator, D. Karoly, A. Kumar, N.-C. Lau, C. Ropelewski, 1998: Progress during TOGA in understanding and modeling global teleconnections associated with tropical sea surface temperatures, *J. Geophys. Res*., **103**(C7), 14291-14324.

Walters, D. N., et al., 2011: The Met Office Unified Model Global Atmosphere 3.0/3.1 and JULES Global Land 3.0/3.1 configurations, *Geosci. Model Dev*., **4**, 919-941.

Wang, B., and X. Xie, 1996: Low-Frequency equatorial waves in vertically shear flow. Part I: Stable waves. *J. Atmos. Sci*., **53**, 449-467.

Wang, B., R. Wu, and X. Fu, 2000: Pacific–East Asian teleconnection: How does ENSO affect East Asian climate? *J. Climate*, **13**, 1517-1536.

Wang, H., and Fu, R., 2000: Winter Monthly Mean Atmospheric Anomalies over the North Pacific and North America Associated with El Niño SSTs. *Am. Meteorol., Soc*., **13,** 3435-3447.

Watanabe, M., and F.-F. Jin, 2002: Role of Indian Ocean warming in the development of Philippine Sea anticyclone during ENSO, *Geophys. Res. Lett*., **29**(10), 1478.

Watanabe, M. and F.-F. Jin, 2003: A moist linear baroclinic model: Coupled dynamical-convective response to El Niño. *J. Climate*, **16**, 1121-1139.

Webster, P. J., and S. Yang, 1992: Monsoon and ENSO: Selectively interactive systems. *Quart. J. Roy. Meteor. Soc*., **118**, 877-926.

Webster, P. J., 1995: The annual cycle and the predictability of the tropical coupled ocean-atmosphere system. *Meteorol. Atmos. Phys*., **56**, 33-55.

Webster, P. J., A. M. Moore, J. P. Loschnigg, and R. R. Leben, 1999: Coupled ocean-atmosphere dynamics in the Indian Ocean during 1997-98. *Nature*, **401**, 356-360.

Wu, R., Z.-Z. Hu, and B. P. Kirtman, 2003: Evolution of ENSO-Related Rainfall Anomalies in East Asia. *J. Climate*, **16**, 3742-3758.

Xie, P., and P. A. Arkin, 1997: Global precipitation: A 17-year monthly analysis based on gauge observations, satellite estimates, and numerical model outputs. *Bull. Amer. Meteor. Soc.*, **78**, 2539-2558.

Xie, S. P., H. Annamalai, F. A. Schott, and J. P. McCreary, 2002: Structure and mechanisms of South Indian Ocean climate variability. *J. Climate*, **15**, 864-878.

Yang, J., Q. Liu, S.-P. Xie, Z. Liu, and L. Wu, 2007: Impact of the Indian Ocean SST basin mode on the Asian summer monsoon. *Geophys. Res. Lett*, **34**, L02708.

Yang, S., and K.-M. Lau, 1998: Influences of Sea Surface Temperature and Ground Wetness on Asian Summer Monsoon. *J. Climate*, **11**, 3230-3246.

Yeh, S.-W., J.-S. Kug and S.-I. An, 2014: Recent progress on two types of El Niño: Observations, Dynamics, and Future changes. Asia-Pacific J. 50, 69-81. (CA)

Yuan, Y., S. Yang, Z. Zhang, 2012: Different Evolutions of the Philippine Sea Anticyclone between the Eastern and Central Pacific El Niño: Possible Effects of Indian Ocean SST. *J. Climate*, **25**, 7867-7883.

Zhou, T., B. Wu, and L. Dong, 2014: Advances in Research of ENSO Changes and the Associated Impacts on Asian-Pacific Climate. *Asia-Pacific J. Atmos. Sci*., **50**(4), 405-422.

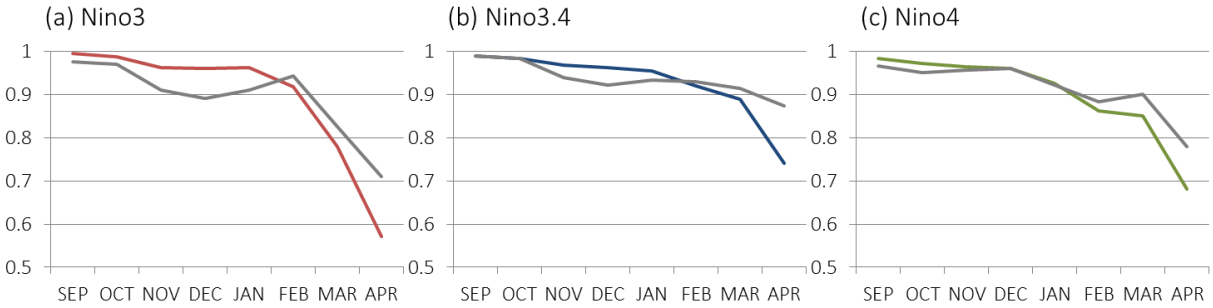

Fig. 1. The correlation coefficients between the observed and predicted Niño SST indices. Gray line denotes the correlation persistence for observed August from 1996-2009. (a) Niño3, (b) Niño3.4 and (c) Niño4, respectively.

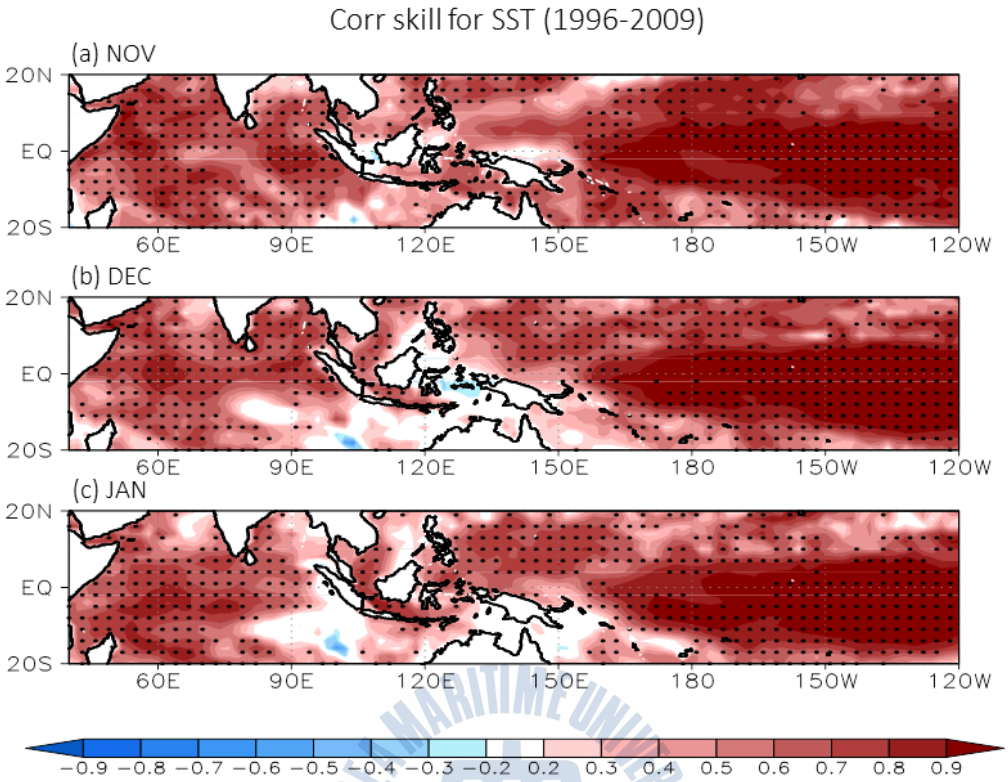

Fig. 2. The correlation coefficients between the observed and predicted SST in (a) November, (b) December and (c) January from 1996-2009. Black dots indicate that the correlation skills is higher than that of the persistence and the correlation 0.3.

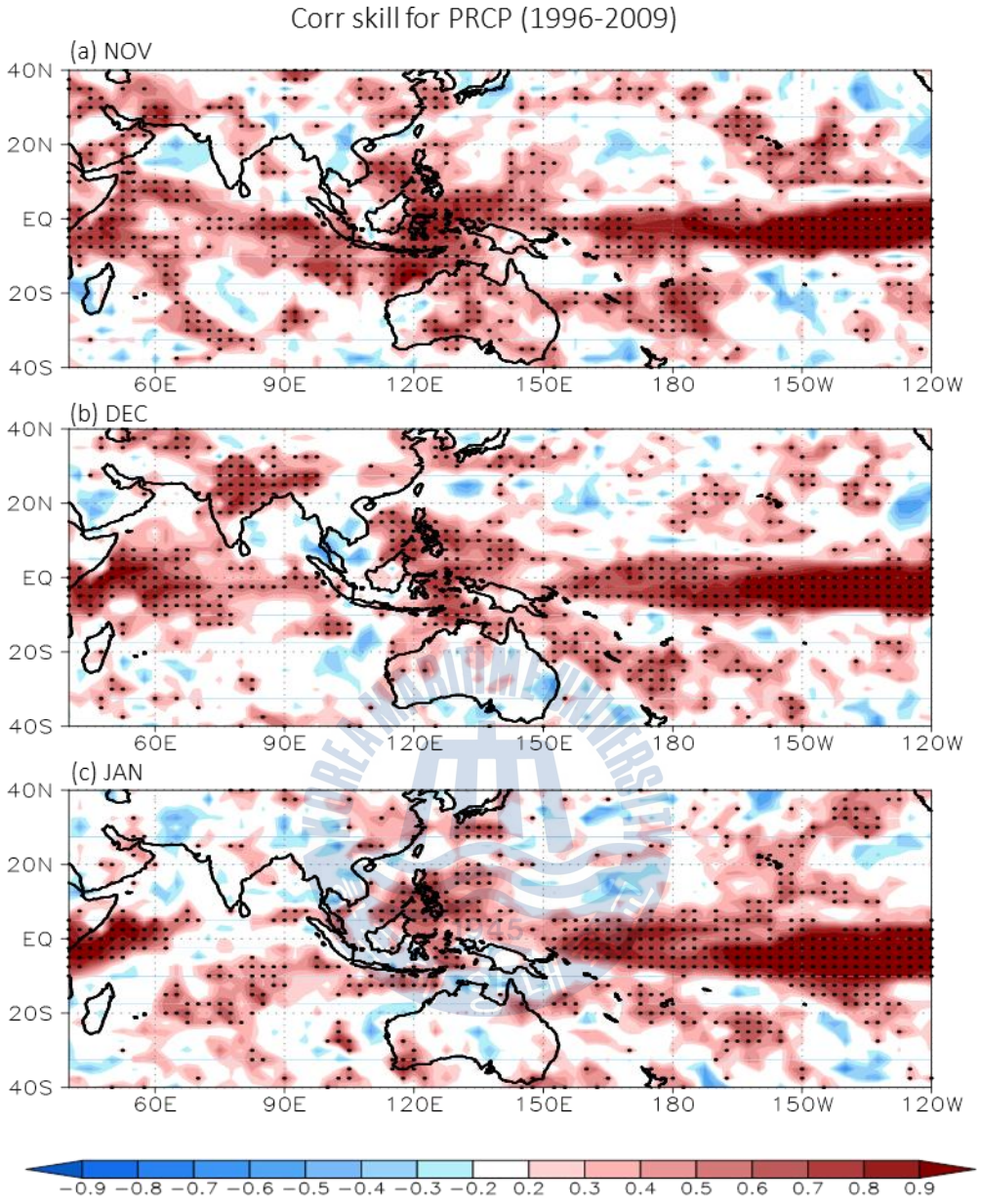

Fig. 3. The same as Fig. 2 except for the precipitation.

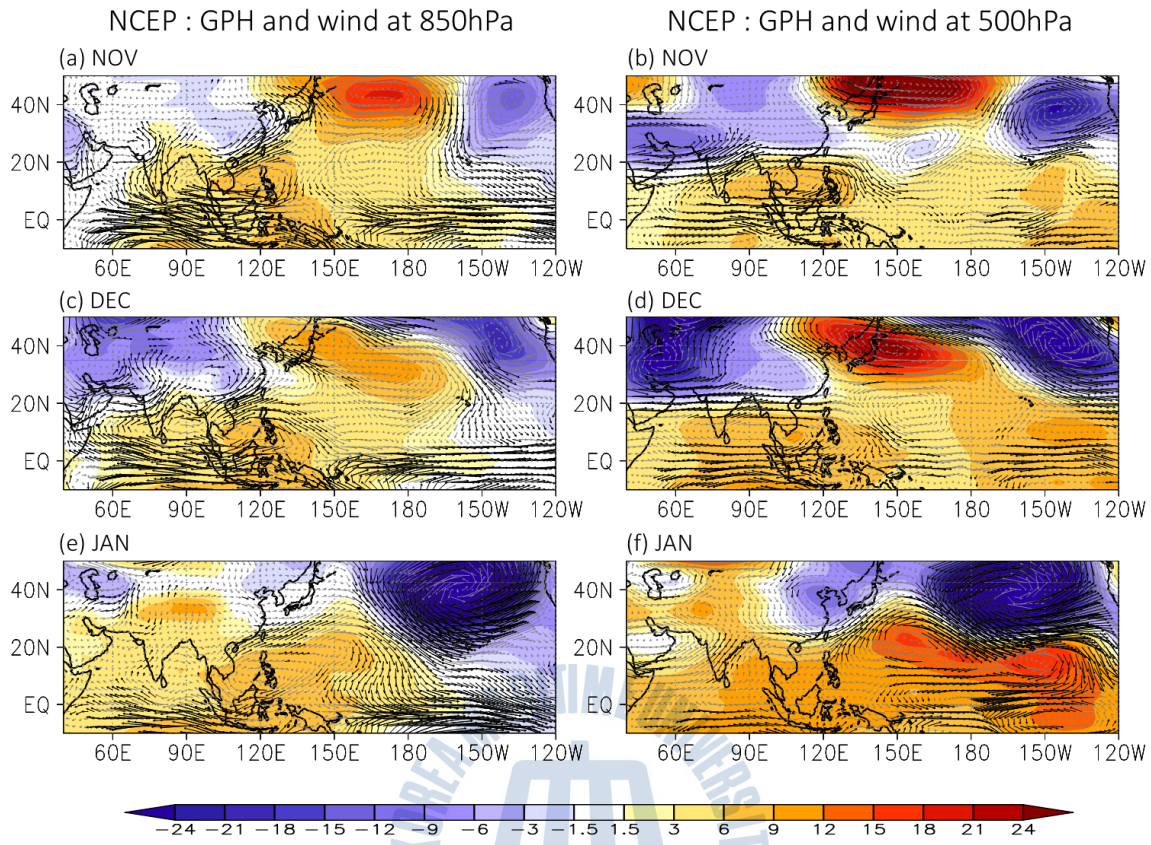

Fig. 4. Regression of 850-hPa geopotential height (shaded; m) and wind (vector; m/s) with respect to Niño3 SST for 850-hPa in (a) November, (c) December and (e) January, and for 500-hPa in (b) November, (d) December and (f) January from 1996-2009. Black wind vector indicates the region exceeding the 90 % confidence level.

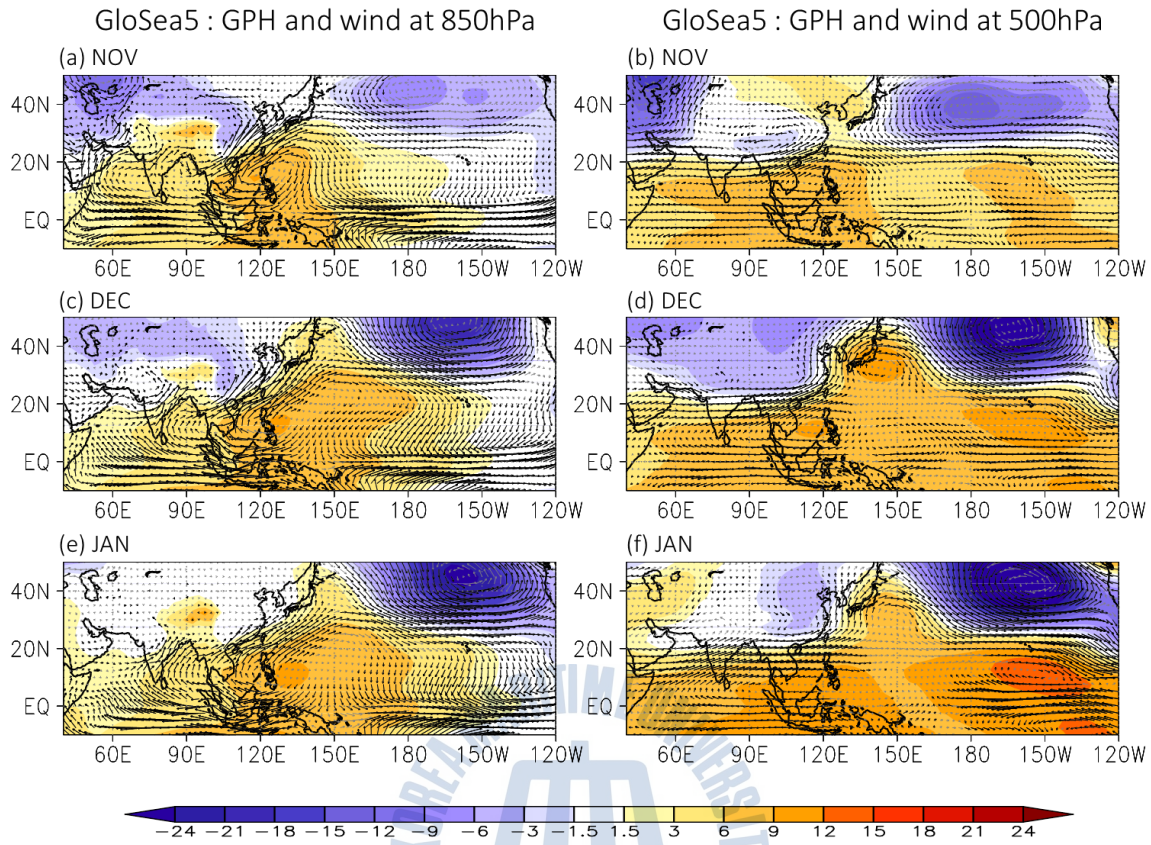

Fig. 5. The same as Fig 4, except for the GloSea5 prediction.

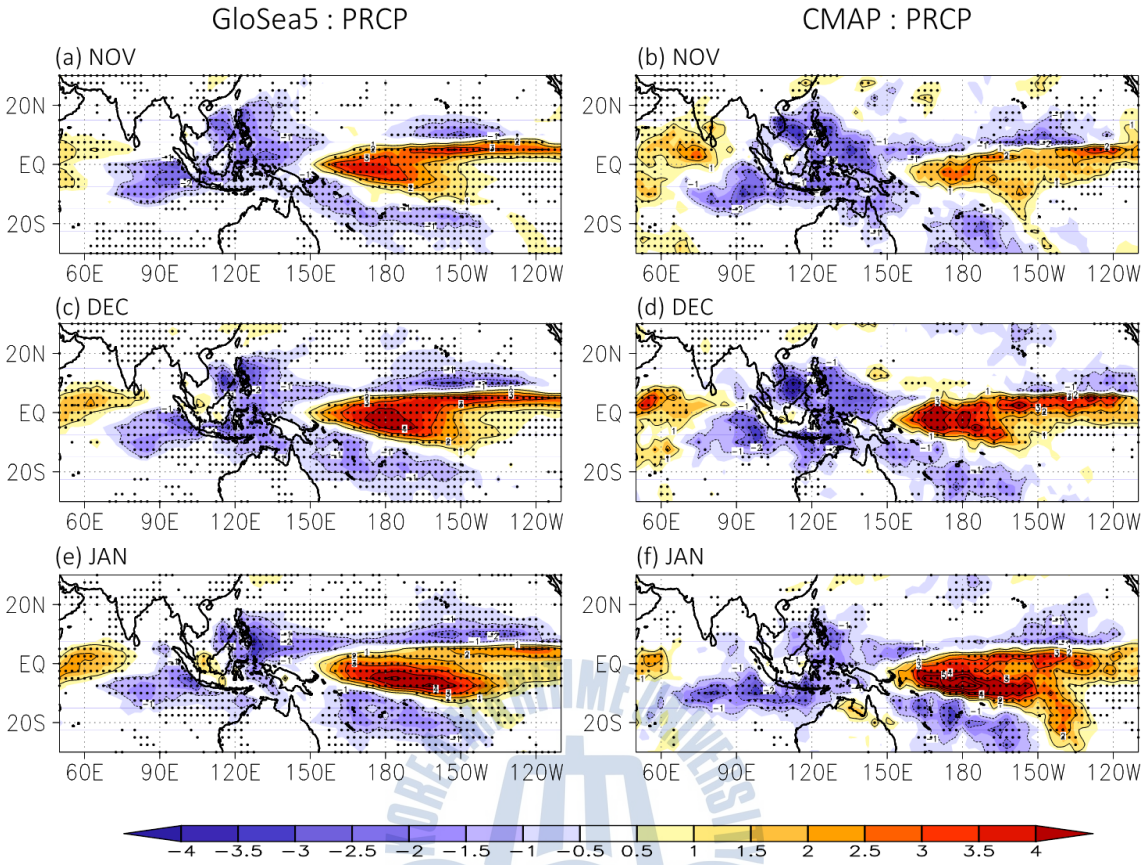

Fig. 6. Linear regression of precipitation with respect to Niño3 SST of the prediction (left panels) and the observation (right panels) in November, December and January during ENSO peak phase for the period of 1996-2009. Black dots indicate the 90 % confidence level.

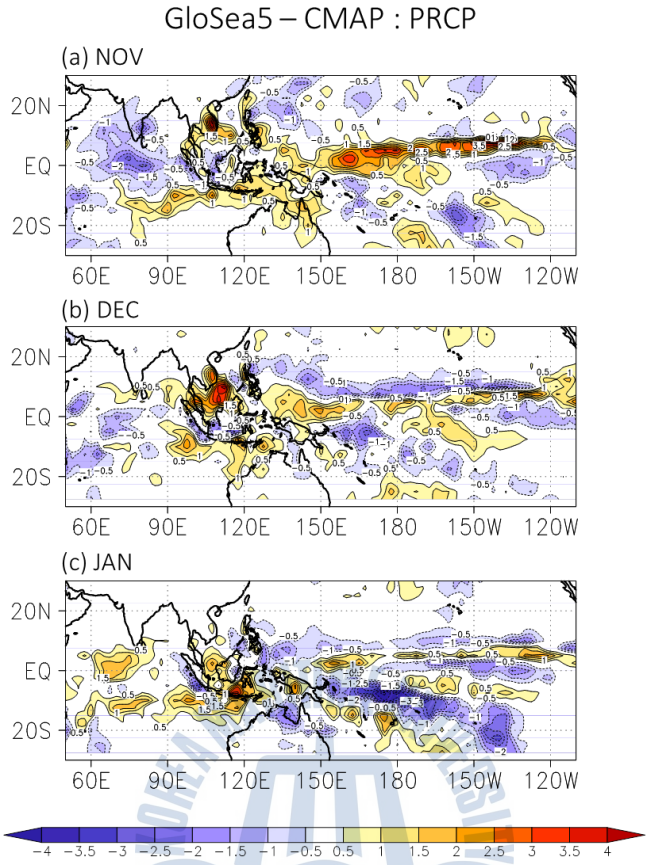

Fig. 7. Difference in GloSea5 and the observation regressed fields of precipitation with respect to Niño3 SST in (a) November, (b) December and (c) January during ENSO peak phase for the period of 1996-2009.

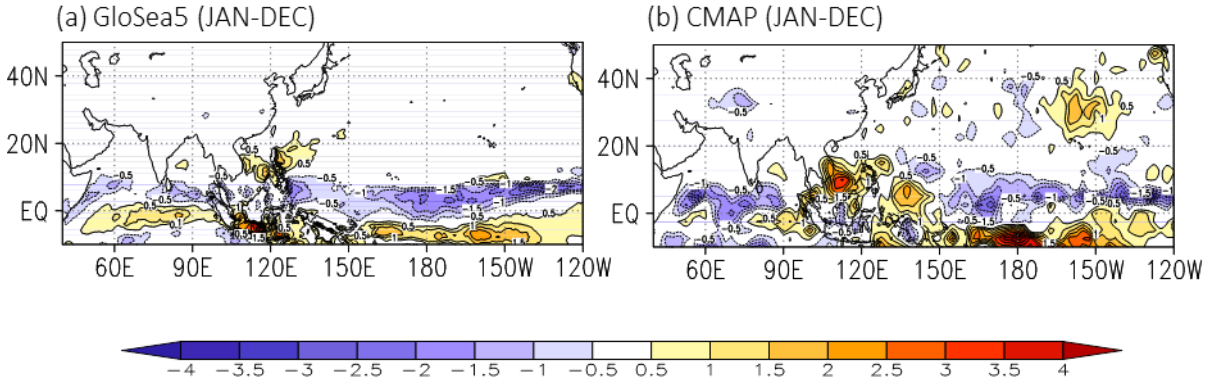

Fig. 8. Difference between January and December regressed field of precipitation with respect to Niño3 SST of the prediction (left panels) and the observation (right panels).

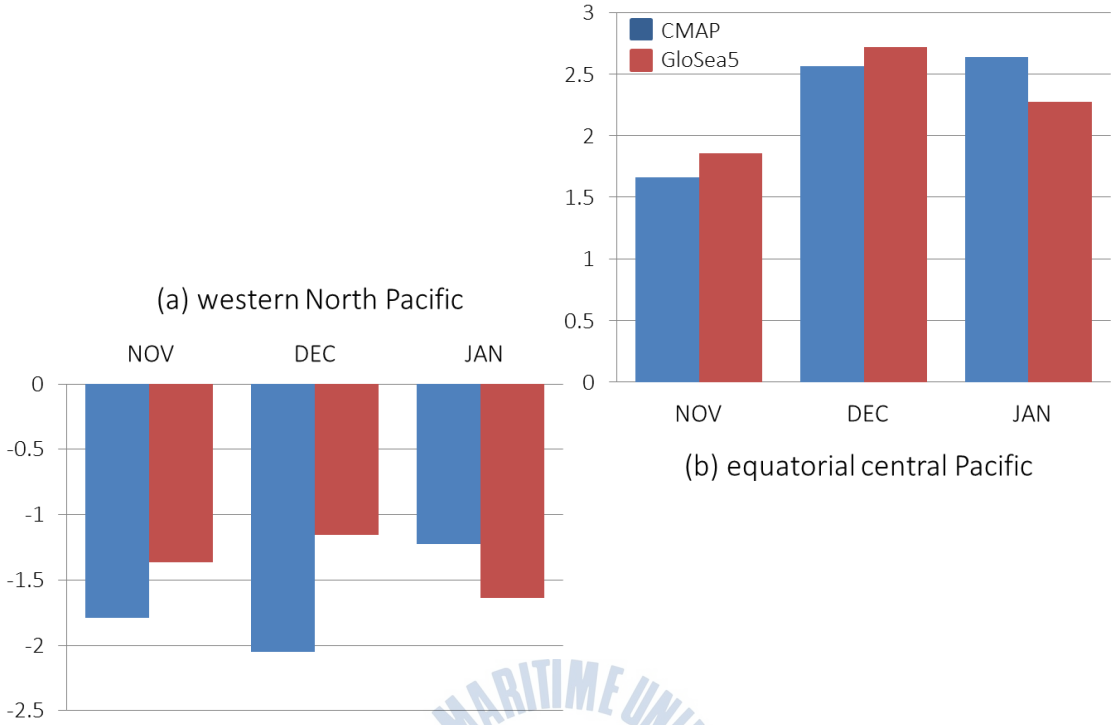

Fig. 9. The area-averaged precipitation regressed with respect to Niño3 SST in November, December and January for the period of 1996-2009 (a) WNP (110 ° E-150 ° E, 0 ° N-10 ° N) and (b) equatorial CP (180 ° E-130 ° W, 5 ° S-5 ° N).

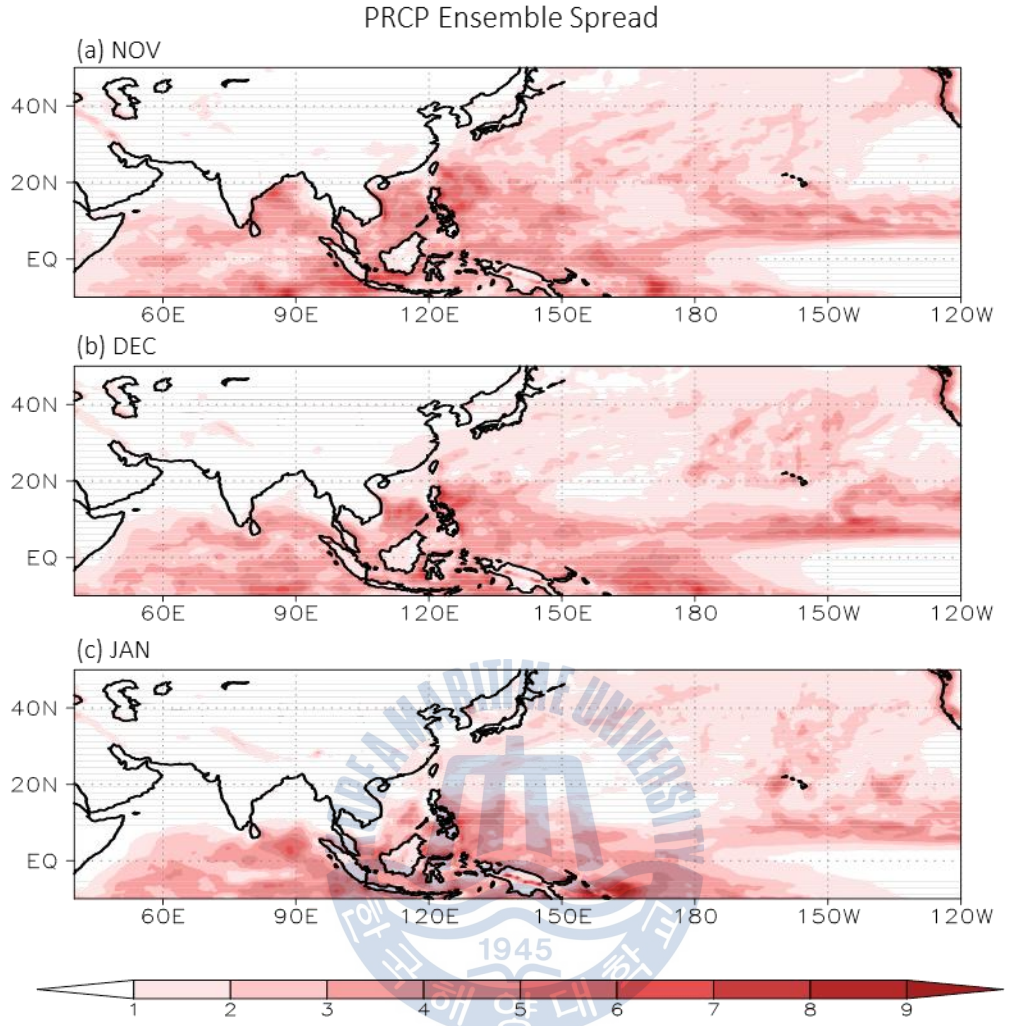

Fig. 10. The precipitation ensemble spread ($mm\ day^{-1}$) between the 12 members of GloSea5 in (a) November, (b) December and (c) January from 1996-2009.

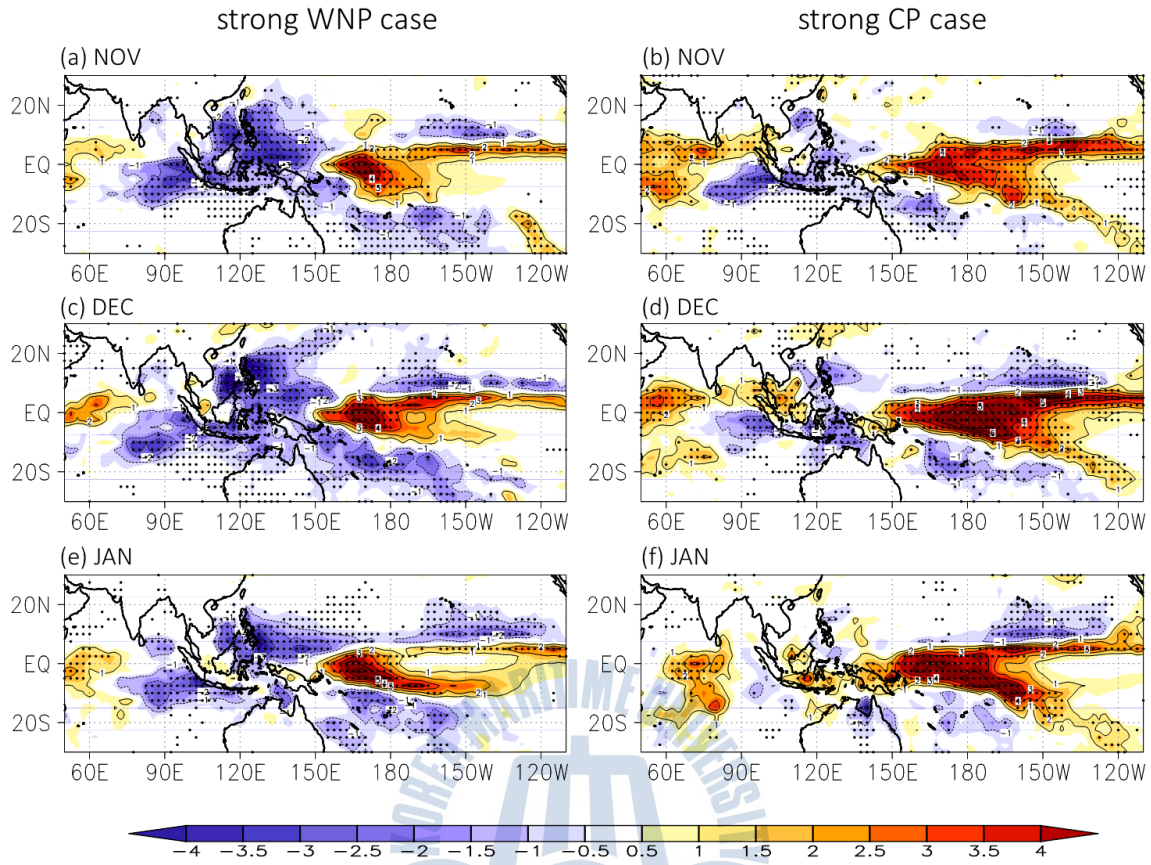

Fig. 11. El Niño composites of precipitation for the strong WNP case (left panels) and strong CP case (right panels) in November, December and January for the period of 1996-2009. Black dots indicate the 90 % confidence level.

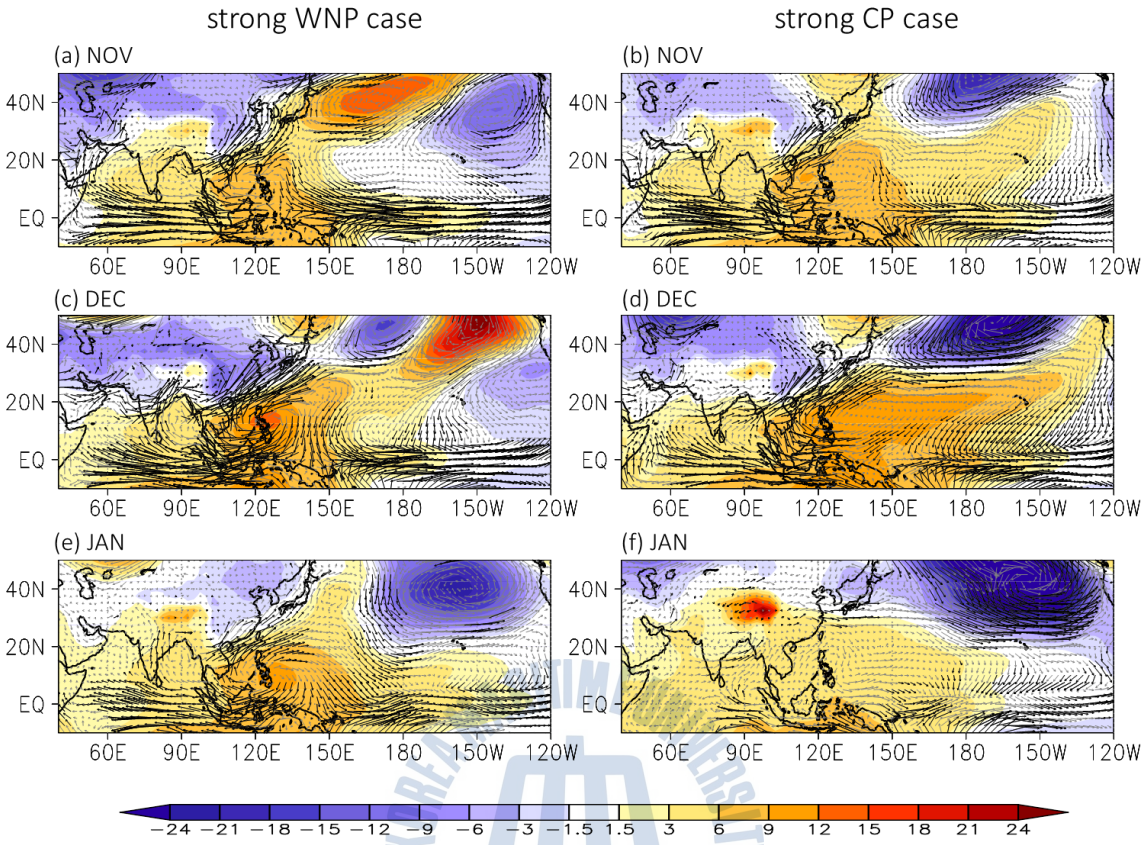

Fig. 12. The same as Fig 11, except for geopotential height and wind at 850-hPa.

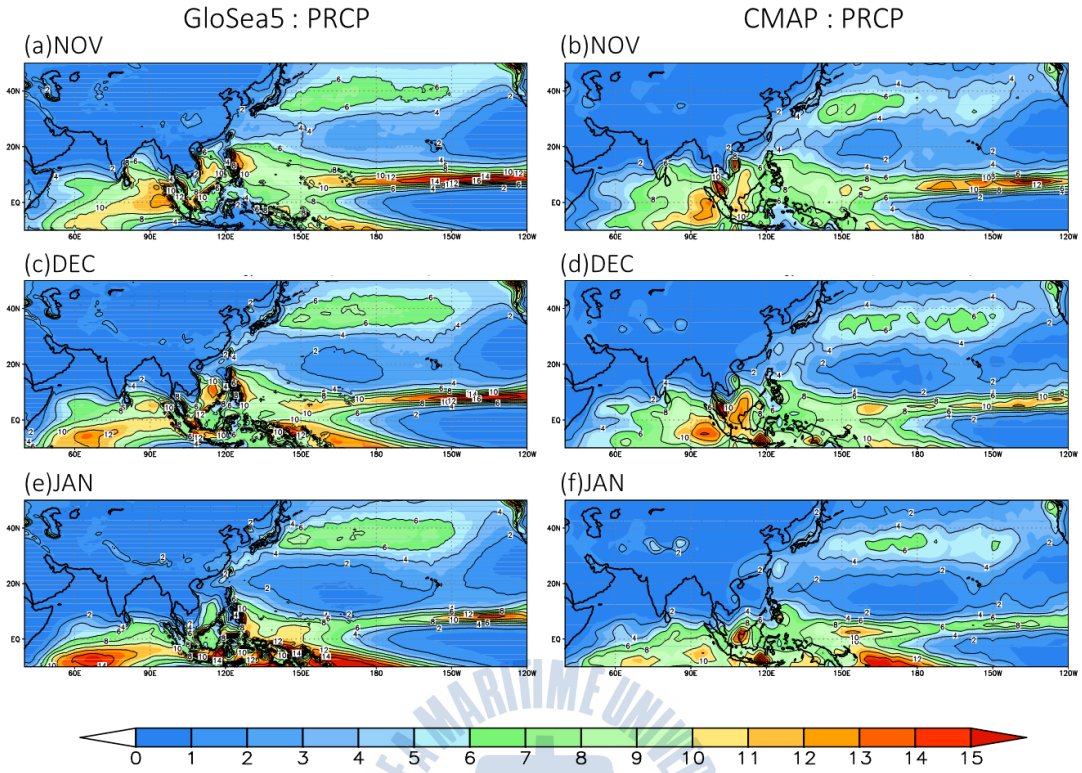

Fig. 13. The monthly mean precipitation climatology of the prediction (left panels) and the observation (right panels) in November, December and January from 1996-2009.

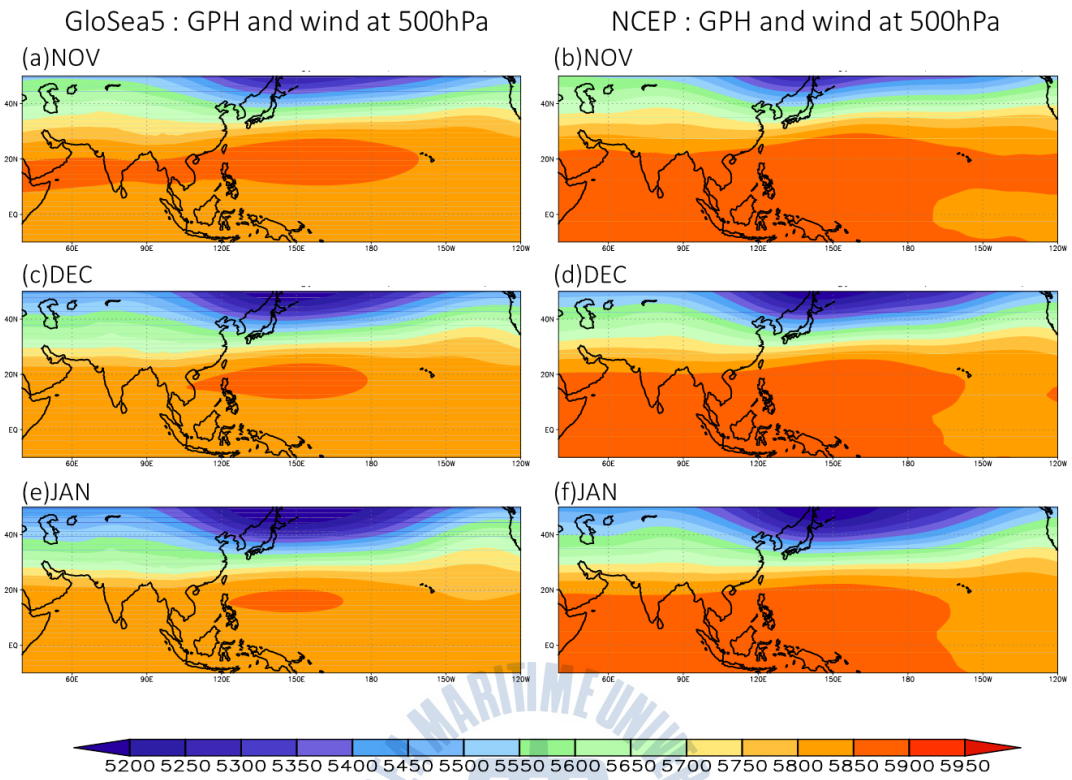

Fig. 14. The same as Fig 13, except for geopotential height and wind at 500-hPa.

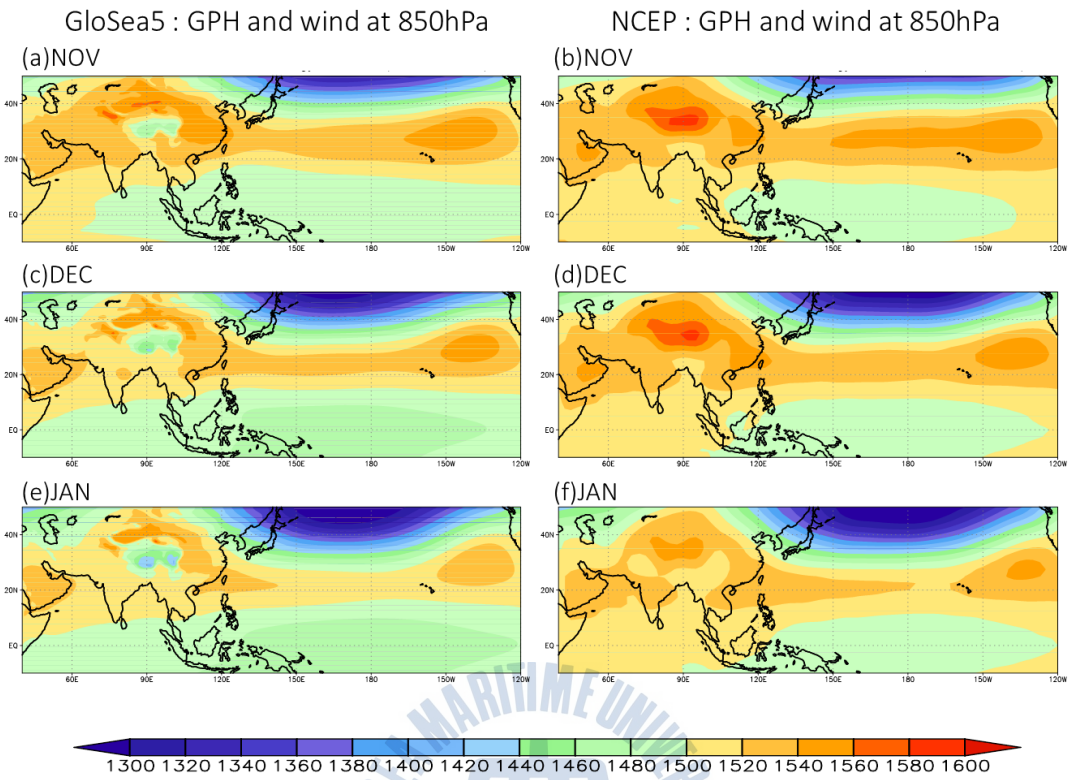

Fig. 15. The same as Fig 14, except for geopotential height and wind at 850-hPa.